



A Coherence Approach to Characterizing Broadband Sound Fields in Ducts

Phillip JOSEPH

Institute of Sound and Vibration Research, University of Southampton, Highfield SO171BJ, UK.

ABSTRACT

This paper describes a new measurement technique that allows the modal amplitude distribution to be determined in ducts with mean flow and reflection based only measurements of the two-point coherence made at the duct wall. The technique is primarily applicable to broadband sound field in the high frequency limit and whose mode amplitudes are incoherent. The technique makes the assumption that the relative mode amplitude distribution is independent of frequency.

Keywords: Duct acoustics, Measurement, Modal analysis.

1. INTRODUCTION

The broadband noise due to fan in a modern turbofan aero engine is one of the dominant noise sources contributing to community noise annoyance, particularly at approach. A detailed understanding of its noise mechanism, an assessment of its sound power transmission, radiation to the far field, and the design of an effective liner to attenuate this noise source, all require detailed measurements of its mode amplitudes. Unlike the noise at the blade passing frequency, which typically comprises just a few dominant modes in accordance with the Tyler Sofrin mode selection rule, broadband noise generally comprises all possible propagating modes. The difficulty with the measurement of their mode amplitudes is that, in general as many microphones are needed to measure the sound field as there is numbers of modes. At frequencies close to the blade passing frequency, for example, the number of modes can readily exceed one hundred, which renders the simultaneous measurement unrealistic. Approaches have been followed to limit the number of microphones by the use of, for example, rotating rakes of microphone arrays where a limited number of microphones are slowly rotated or traversed though the in-duct sound field. Modal amplitudes may then be deduced though the inversion of the cross spectral pressure matrix. Very often, however, the matrix to be inverted can become ill-conditioned leading to erroneous mode amplitude estimates.

A pragmatic solution to determining the mode amplitude distribution in ducts has been proposed by Lewis et al in which a single axial array of microphones at the duct wall are used as a beamformer to estimate the in-duct noise directivity. Rather than providing information about the mode amplitude for the different mode orders (m,n) , the technique provides information about the distribution of mode amplitudes versus in-duct propagation angle. For the intended applications listed above, this limitation presents no difficulty as it has long been recognized that modes with the propagation angles possess near identical transmission and radiation characteristics¹.

2. MODAL TRANSMISSION

Consider a hard-walled cylindrical duct of finite-length, as sketched in Fig 1 below, containing an axial uniform mean flow moving in the positive x direction with flow speed cM ($M > 0$), where c is the sound speed and M is the mean flow Mach number. A point on the duct cross section is represented by $\mathbf{y} = (r, \theta)$ and x denotes the axial distance along the duct relative to some arbitrary origin. Two microphones mounted flush to the duct wall, separated axially by a distance Δx , are used to detect the acoustic pressure. The objective here is to deduce the distribution of mode amplitudes in the duct using the acoustic pressure information at the two microphones.

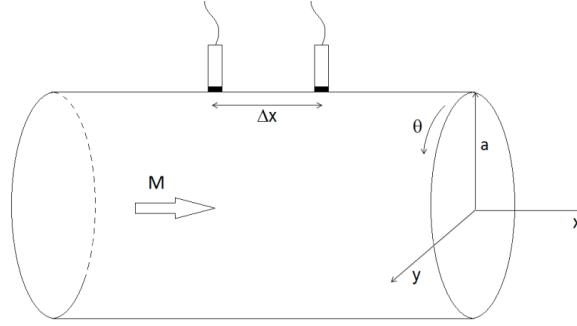


Figure 1. Semi-infinite, hard walled unflanged circular duct with associated co-ordinate system. Two microphones mounted flush to the duct wall, separated axially by a distance Δx , are used to detect the acoustic pressure.

The sound field $p(x, \mathbf{y})$ in the duct satisfies the convected homogeneous wave equation,

$$\left(\frac{1}{c^2} \frac{\bar{D}^2}{Dt^2} - \nabla^2 \right) p = 0 \quad (1)$$

where $\frac{\bar{D}}{Dt} = \frac{\partial}{\partial t} + c M \frac{\partial}{\partial x}$ is the convected derivative operator associated with the mean flow velocity $(cM, 0, 0)$ in the (x, \mathbf{y}) coordinate system and c is the sound speed in the quiescent medium. Above its cutoff frequency, at a single frequency ω , a single mode of pressure amplitude A_{mn} is described by

$$p_{mn}^{\pm}(\mathbf{y}, x) = e^{-i\omega t} A_{mn}^{\pm} \Psi_{mn}(\mathbf{y}) e^{ik_{mn}^{\pm} x} \quad (2)$$

where the superscript '+' refers to modes propagating in the direction of flow and '-' to modes propagating in the opposite direction to the flow. Equation (2) in Eq. (1) gives

$$k_{mn}^{\pm} = \left(\frac{\pm \alpha_{mn} - M}{\beta^2} \right) \frac{\omega}{c}, \quad \alpha_{mn} = \sqrt{1 - (\kappa_{mn}/k)^2 \beta^2}. \quad (3a,b)$$

where $\beta^2 = (1 - M^2)$ and κ_{mn} are a set of eigenvalues that are characteristic of the duct cross section such that the corresponding mode shape functions Ψ_{mn} , defined by $(\nabla^2 + \kappa_{mn}^2) \Psi_{mn}(\mathbf{y}) = 0$, also satisfy the duct-wall boundary conditions and the normalization condition $A^{-1} \int |\Psi_{mn}(\mathbf{y})|^2 dA(\mathbf{y}) = 1$. The parameter α , which we shall call the cut-on ratio, is central in what follows, and takes values between $\alpha = 0$ precisely at the modal cutoff frequency $\omega = \omega_{mn} = \kappa_{mn} c (1 - M^2)^{\frac{1}{2}}$, and tends to $\alpha = 1$ as $\omega/\omega_{mn} \rightarrow \infty$, corresponding to modes well above cuton. Modes propagating in the direction of the flow are represented by $\alpha \geq 0$ while modes propagating in the opposite direction (against the flow) are represented by, $\alpha \leq 0$.

The in-duct sound field at any position in the duct cross section $\mathbf{y} = (r, \theta)$, axial position x , and frequency ω , can be expressed as the sum of modal components propagating in the direction of flow p_{mn}^+ , and modes propagating opposite to the direction of flow p_{mn}^- ,

$$p(\mathbf{y}, x) = \sum_{m=-\infty}^{\infty} \sum_{n=0}^{\infty} [p_{mn}^+(\mathbf{y}, x) + p_{mn}^-(\mathbf{y}, x)], \quad (4)$$

where (m, n) are the usual circumferential and radial mode indices².

3. RELATIONSHIP BETWEEN MODE AMPLITUDE DISTRIBUTION AND COHERENCE

The acoustic pressure cross spectrum between two points separated axially along the duct wall $\mathbf{y}_a = (r = a, \theta)$, at axial distances x_1 and $x_1 + \Delta x$, may be written as

$$S_{12}(\omega, \mathbf{y}_a, x_1, x_2) = \frac{\pi}{T} E \left\{ p(\mathbf{y}_a, x_1) p^*(\mathbf{y}_a, x_1 + \Delta x) \right\} \quad (5)$$

where $E\{\}$ denotes the expectation and the acoustic pressures refer to Fourier Transforms of the pressure time series taken over a time duration T . For incoherent excitation of the sound field we treat the mode amplitudes as uncorrelated random variables so that $E\{A_{mn} A_{m'n'}^*\} = 0$. We further assume that the same mode propagating in opposite directions are also uncorrelated such that, $E\{A_{mn}^+(\omega) A_{mn}^-(\omega)^*\} = 0$. Substituting Eqs (2) and (4) into Eq (5) and invoking the uncorrelated mode assumptions above leads to,

$$S_{12}(\omega, \mathbf{y}) = \sum_{m,n} \left[E \left\{ |A_{mn}^+(\omega)|^2 \right\} e^{ik_{mn}^+ \Delta x} + E \left\{ |A_{mn}^-(\omega)|^2 \right\} e^{ik_{mn}^- \Delta x} \right] \Psi_{mn}^2(\mathbf{y}) \quad (6)$$

Work by Rice³, and more recent work by Joseph et al⁴, have shown that there are a physically important class of source distributions for which the *relative* mode amplitude distribution is *independent* of frequency and only a function of the cut off ratio α_{mn} (equivalently, mode propagation angle¹, see equation (25) below). Well known examples include a uniform distribution of monopole sources, axial dipole sources and equal energy per mode⁴. In these, and many other source distributions, we may write,

$$E \left\{ |A_{mn}^\pm(\omega)|^2 \right\} = S(\omega) \overline{a_\pm^2}(\alpha_{mn}) \quad (7)$$

where $S(\omega)$ is the frequency-dependent source strength with dimensions of pressure squared per unit frequency and $\overline{a_\pm^2}(\alpha_{mn})$ specifies the relative distribution of non-dimensional mean square mode amplitudes, which depends only on α_{mn} . A list of some physically important examples are listed in the Appendix. The assumption of the separability of $E \left\{ |A_{mn}^\pm(\omega)|^2 \right\}$ into a purely frequency-dependent term $S(\omega)$ and a mode distribution term $\overline{a_\pm^2}(\alpha_{mn})$ (which controls the spatial variation of the sound field) is central to the validity of the technique. The split between the two terms in Eq. (7) is essentially arbitrary. For reasons that will become clear below, we define $\overline{a_\pm^2}(\alpha_{mn})$ with the normalization property,

$$\sum_{m,n} \left[\overline{a_+^2}(\alpha_{mn}) + \overline{a_-^2}(\alpha_{mn}) \right] = 1 \quad (8)$$

We now denote the amplitude of waves propagating against the direction of flow (i.e., reflected modes in this case) by negative argument α so that

$$\begin{aligned} \overline{a_+^2}(\alpha_{mn}) &= \overline{a^2}(\alpha_{mn}), & \alpha &\geq 0 \\ \overline{a_-^2}(-\alpha_{mn}) &= \overline{a^2}(\alpha_{mn}), & \alpha &\leq 0 \end{aligned} \quad (9)$$

In the high frequency limit ($ka = \omega a/c > 10$ has been found to be sufficient, where a is the duct radius), we may treat $\overline{a^2}(\alpha)$ as a continuous variable so that the discrete summation over $\overline{a^2}(\alpha_{mn})$ in Eq. (6) may be replaced by an integration over α . The normalization condition of Eq. (8) may therefore be written as

$$\int_{-1}^1 \overline{a^2}(\alpha) n(\alpha) d\alpha = 1 \quad (10)$$

where $n(\alpha)$ the modal density function introduced to take account the distribution of modes across their range of α -values, defined by,

$$n(\alpha) = \frac{N(\alpha + \delta\alpha) - N(\alpha)}{N\delta\alpha} \Big|_{\lim \delta\alpha \rightarrow 0}, \quad \int_{-1}^1 n(\alpha) d\alpha = 1 \quad (11a,b)$$

where $N(\alpha)$ is the number of modes with ' α ' values of between -1 and α and N is the total number of propagating modes at frequency ka , i.e., $N = \int_{-1}^1 N(\alpha) d\alpha$. Rice has shown that in a cylindrical duct with uniform mean flow, the total number of propagating modes N takes the high-frequency limiting value³,

$$N \rightarrow \left(\frac{1}{2} ka / \beta\right)^2, \quad ka / \beta \rightarrow \infty \quad (12)$$

Following Rice¹, and re-expressed in terms of cuton ratio α by Joseph et al^{4,5}, the high- ka asymptotic density function n , is given by,

$$n(\alpha) = |\alpha| \quad (13)$$

Note that Eq. (13) differs by a factor of $1/2$ from the expression originally presented by Joseph et al⁴, which assumes a distribution a modes propagating from *one direction* only. Equation (13) indicates a scarcity of modes that are just cut-on ($\alpha \approx 0$) compared with a higher population of modes that are well cut on, ($|\alpha| \approx 1$).

Simplifications to Eq. (6) for the pressure cross spectrum at the duct wall are obtained by replacing $\Psi_{mn}^2(\mathbf{y})$ by its average value at the duct wall⁴, averaged over all values of mode indices m and n ,

$$\Psi_{mn}^2(\mathbf{y}) = \langle \Psi^2(\mathbf{y}) \rangle_{mn} = 2. \quad (14)$$

Taking the average incurs greatest error for modes with the largest m values whose values of $\Psi_{mn}^2(\mathbf{y})$ are concentrated at the duct wall. These modes are comparatively scarce, however (with $m = 0$ having the largest number of radial modes and hence being most common), and hence the approximation of Eq. (14) introduces negligible error compared with the exact calculation of Eq. (6). Substituting Eq. (7) for $|A_{mn}(\omega)|^2$, Eq. (3a) for k_{mn} , and taking the high frequency limit in the sense of Eq. (10), leads to an integral expression for the pressure cross spectrum $S_{12}(\omega, \mathbf{y}_a, \Delta x)$ between two microphones separated axially by a distance Δx at the duct wall $\mathbf{y}_a = (a, \theta)$ involving only the cutoff ratio and the frequency-dependent source strength,

$$\frac{S_{12}(\hat{\omega}, \mathbf{y}_a)}{S(\hat{\omega})} = 2N e^{-iM\hat{\omega}} \int_{-1}^1 \frac{1}{a^2}(\alpha) n(\alpha) e^{i\hat{\omega}\alpha} d\alpha, \quad (15)$$

which is a function only of the non-dimensional frequency, $\hat{\omega}$

$$\hat{\omega} = \omega \Delta x / c\beta^2, \quad (16)$$

Note that the source term $S = S(\hat{\omega})$ has also been written as a function of $\hat{\omega}$ which is permissible since S is a source term and therefore unrelated to Δx and so there is no difficulty in non-dimensionalising the source frequency ω with respect to this arbitrary distance. A consequence of making the separability assumption of Eq. (7) is that the cross spectrum is only a function of the non-dimensional frequency, $\hat{\omega}$. Thus, cross spectra measured at the duct wall for different separation distances Δx , plotted against $\hat{\omega}$, should collapse provided that this separability assumption is met. This property therefore provides a simple test of the validity of Eq. (7). In practice, however, the coherence measurement will be affected by non-acoustic pressure contributions from flow noise at the microphones. In practice, therefore, steps should be taken to minimize contamination by flow noise by, for example, recessing the microphones into the duct wall.

Interpretation of S.

Putting $\Delta x = 0$ in Eq (6) yields the pressure Power Spectral Density $S_{11}(\omega, \mathbf{y})$ at any point over the duct cross section \mathbf{y} . Averaging the result over the duct cross section area A and taking the high frequency limit yields,

$$\left[\frac{1}{A} \int_S S_{11}(\hat{\omega}, \mathbf{y}) dS(\mathbf{y}) \right]_{f \rightarrow \infty} = S(\hat{\omega}) N \left[\int_{-1}^1 \overline{a^2(\alpha)} n(\alpha) d\alpha \right] \left[\frac{1}{A} \int_A \Psi_{mn}^2(\mathbf{y}) dS(\mathbf{y}) \right] \quad (17)$$

Noting the normalization property of the mode shape functions, $A^{-1} \int_S \Psi_{mn}^2(\mathbf{y}) dS(\mathbf{y}) = 1$ and the mode amplitude normalization property of Eq. (10), Eq. (17) reduces to,

$$S(\hat{\omega}) = \left[\frac{1}{N} \frac{1}{A} \int_S S_{11}(\hat{\omega}, \mathbf{y}) dS(\mathbf{y}) \right]_{f \rightarrow \infty} \quad (18)$$

The source strength $S(\hat{\omega})$ therefore has the interpretation as the high frequency noise pressure spectrum averaged over the duct cross sectional area, per mode. Joseph et al⁴ has shown that, in the high frequency limit, the pressure PSD averaged over the duct cross section, $NS(\hat{\omega})$, is half the pressure Power Spectral Density (PSD) measured at the duct wall $S_{11}(\hat{\omega}, \mathbf{y}_a)$, i.e.,

$$S_{11}(\hat{\omega}, \mathbf{y}_a) = 2NS(\hat{\omega}) \quad (19)$$

Substituting Eq. (19) into (15) leads to,

$$S_{12}(\hat{\omega}) = S_{11}(\hat{\omega}) e^{-iM\hat{\omega}} \int_{-1}^1 \overline{a^2(\alpha)} |\alpha| e^{i\hat{\omega}\alpha} d\alpha \quad (20)$$

In Eq. (20), and all future results, the dependence on \mathbf{y}_a is dropped since it is now understood that *all* measurements are made at the duct wall. Finally we make the approximation that $S_{11}(\hat{\omega}) \approx S_{22}(\hat{\omega})$ and hence $S_{11}(\hat{\omega}) \approx \sqrt{S_{11}(\hat{\omega})S_{22}(\hat{\omega})}$, since Δx is usually very small (typically a few centimeters), and set the upper limit of integration to infinity (since $\overline{a^2(\alpha)} \approx 0$ for $|\alpha| > 1$ corresponding to cutoff modes). The final result is,

$$\psi_{12}(\hat{\omega}) = e^{-iM\hat{\omega}} \int_{-\infty}^{\infty} \overline{a^2(\alpha)} |\alpha| e^{i\hat{\omega}\alpha} d\alpha \quad (21)$$

Equation (21) represents a Fourier Transform relationship between the α – weighted normalized mode amplitude distribution function $\overline{a^2(\alpha)}$ and the complex coherence function $\psi_{12}(\hat{\omega})$,

$$\psi_{12}(\hat{\omega}) \approx \frac{S_{12}(\hat{\omega})}{\sqrt{S_{11}(\hat{\omega})S_{22}(\hat{\omega})}} \quad (0 \leq |\psi_{12}(\hat{\omega})|^2 \leq 1) \quad (22)$$

The mean square mode amplitude distribution, with the normalization property of Eq (8), may therefore be readily deduced from the inverse Fourier Transform of the complex coherence function weighted by $e^{iM\hat{\omega}}$.

$$\overline{a^2(\alpha)} = \frac{1}{2\pi|\alpha|} \int_{-\infty}^{\infty} \psi_{12}(\hat{\omega}) e^{iM\hat{\omega}} e^{-i\hat{\omega}\alpha} d\hat{\omega} \quad (23)$$

Equation (23) is the main result of this paper. It suggest that the normalized mode amplitude distribution may in principle be deduced using just two microphones for any incoherent multi-mode sound field whose cross spectra collapses on the non-dimensional frequency $\hat{\omega} = \omega\Delta x/c\beta^2$. The phase factor $e^{iM\hat{\omega}}$ serves as a Lorentz transformation into the reference frame moving with the flow such that the amplitude distribution

for right and left-traveling propagating modes is now symmetric in α , lying in the range $-1 \geq \alpha > -1$.

In this section we validate the principles set out above by a number of numerical examples to illustrate the effectiveness of the technique in deducing, based only on the complex coherence measurement at the duct wall, the mode amplitude distribution and transmitted sound power for incident and reflected modes, and the far field pressure directivity. We consider the idealized case of a duct in which all the modes propagating towards the end of the duct contain equal sound power. The normalized mode amplitude distribution is obtained by setting $W_0 = 1$ in Eq. (28) and normalizing according to Eq. (11b),

$$\overline{a^2}(\alpha) = \frac{(1 - \alpha M)^2}{\alpha(1 + M^2/3)} \quad (36)$$

In a hard walled cylindrical duct the mode shape function are of the form $|\Psi_{mn}(r)| = |J_m(k_{r_{mn}} r)| / \Gamma_{mn}$, where J_m are Bessel functions of the 1st kind or order m , $k_{r_{mn}}$ is the n^{th} stationary value of J_m and Γ_{mn} are constants chosen to satisfy the normalisation condition presented above. Modal pressure reflection coefficients of the form $R(\alpha) = \exp(-\delta\alpha/2)$ are assumed in the simulations, so that $a_-^2(\alpha) = R^2(\alpha)a_+^2(\alpha)$, where δ specifies the rate at which the reflection coefficient diminished as the modes is excited well above cut off. This reflection coefficient model is consistent with other more accurate models and is designed to ensure that modes at cutoff, $\alpha = 0$, are perfectly reflected, with the reflection coefficient reducing as the modes become increasing cuton as frequency is increased¹.

Special cases; zero Mach number, arbitrary reflection

We first consider the case of $M = 0$ since it allows analytic expression to be derived and compared against exact numerical predictions. For the case of Equal energy per Mode, the mode amplitude distribution may be obtained by setting the sound power in each mode equal to unity, $W_{mn}^+(\omega) = W_0 = 1$ in Eq. (28),

$$\overline{a^2}(\alpha) = \begin{cases} 1/\alpha N & \alpha \geq 0 \\ \exp(-\delta\alpha)/(|\alpha|N) & \alpha \leq 0 \end{cases} \quad (37)$$

where N is the factor designed to ensure that $\overline{a^2}(\alpha)$ is correctly normalized according to Eq. (10) and equals, $N = (1 + \delta - e^{-\delta})/\delta$. The complex coherence function is obtained from substituting Eqs (37) into (21) to give

$$\psi_{12}(\hat{\omega}) = \frac{\delta}{1 + \delta - e^{-\delta}} \left[\frac{e^{-\delta/2} e^{-\frac{1}{2}i\hat{\omega}} \left[\sin \frac{1}{2} \hat{\omega} \cosh \frac{1}{2} \delta - i \cos \frac{1}{2} \hat{\omega} \sinh \frac{1}{2} \delta \right]}{\frac{1}{2} (\hat{\omega} - i\delta)} + \frac{e^{\frac{1}{2}i\hat{\omega}} \sin(\frac{1}{2} \hat{\omega})}{\frac{1}{2} \hat{\omega}} \right] \quad (38)$$

Figures 2a and 2b show a comparison of the coherence magnitude and phase respectively, evaluated at the duct wall for an equal energy per mode sound field computed from the exact modal summation of Eqs. (6 and 22) (blue curve) with the analytic expression of Eq. (38) (black dashed curve). Comparison are shown for the four reflection factors, $\delta = 0, 1, 2$ and 5 . Note that the curves have been separated for ease of readability.

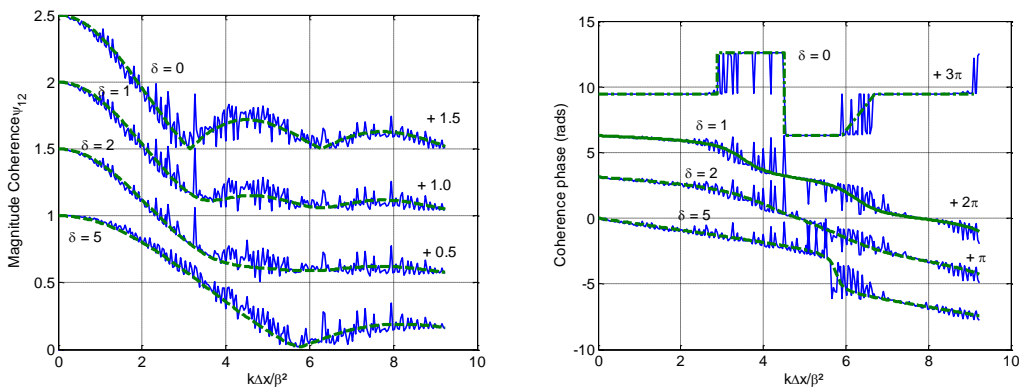


Figure 2. Comparison of 'exact' and theoretical coherence function magnitude and phase for $M = 0$ at different levels of reflectivity, $\delta = 0, 1, 2$ and 5 . Note that the curves have been separated for ease of viewing.

Oscillations in the exact calculation arise from the behavior of the spectra at the modal cuton frequencies. Here the pressure amplitude tends to infinity as the cutoff frequency is approached. As the modal reflectivity is increased (by reducing δ) the coherence magnitude and phase both exhibit greater variability.

Limiting cases case of the coherence function may be obtained for the case of perfect modal reflectivity $\delta = 0$, and when the reflectivity is zero, i.e., the duct may be assumed to infinite. In the latter case, putting $\delta \rightarrow \infty$ into Eq. (38) yields

$$\psi_{12}(\hat{\omega}) \rightarrow \exp\left(\frac{1}{2}i\hat{\omega}\right) \frac{\sin\left(\frac{1}{2}\hat{\omega}\right)}{\frac{1}{2}\hat{\omega}} \tag{39}$$

which is in close agreement with the exact calculation shown in figures 2a and 2b. The ducted sound field may now be regarded as a one-sided (or hemi-diffuse sound field). The phase delay between the two microphones which varies with frequency as $\frac{1}{2}\omega\Delta x/c$, i.e., precisely half the rate of a purely plane wave. Precisely this behavior is observed in figure 2a and b for the case of least reflectivity, $\delta = 5$. When all modes are perfectly reflected at the end of the duct, $\delta \rightarrow 0$, and Eq. (38) tends to

$$\psi_{12}(\hat{\omega}) \rightarrow \frac{\sin\hat{\omega}}{\hat{\omega}} \tag{40}$$

In this case, where each incident has equal sound power and is perfectly reflected incoherently, the coherence function is identical to that of a diffuse sound field in which energy is arriving from all angles equally. Clearly, therefore, there is no phase variation between the two microphones, as shown in figure 2b, where 2π phase jumps can be observed due to unwrapping issues.

Mode amplitude distribution

Figure 3 shows a comparison of the exact mean square mode amplitude distribution versus α of Eq. (37) with that deduced by inversion of the complex coherence functions plotted in figures 2 by the use of Eq. (23).

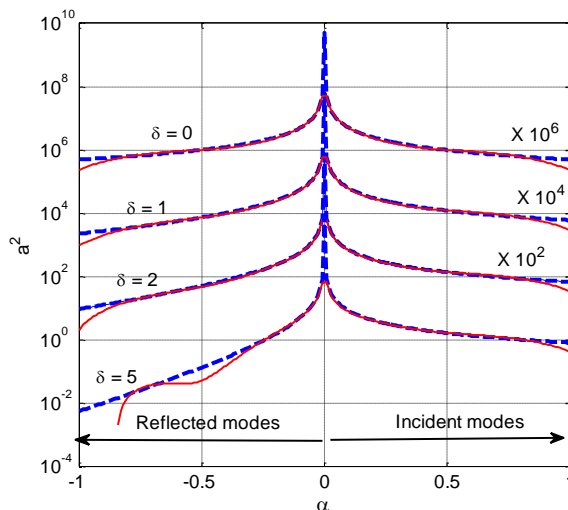


Figure 3. Comparison of the exact (blue curves) and inverted mode amplitude distribution (red curves) for four reflectivity factors at $M = 0$.

Agreement between the exact and inverted mode amplitude distribution is generally excellent except near the extreme value of $\alpha = 0$, where the modes are well cuton, and $|\alpha| = 1$, corresponding to modes that are close to cutoff. Errors are particularly great for the very well cuton modes. This is likely to be due to the choice of ‘equal energy per mode’ model chosen for the simulation since the mode distribution becomes singular at $\alpha = 0$, which clearly cannot be recovered from Eq. (23) using a numerical integration. Errors are also pronounced for the near-cutoff modes particularly for the case of least reflectivity arising from numerical errors in the evaluation of Eq. (23).

4. EXPERIMENTAL APPLICATION

We now apply the mode amplitude measurement technique to some coherence data obtained in the bypass section of the Anecom fan rig at Germany, shown below in figure X. The mean flow Mach number was 0.247. The microphones were mounted flush to the duct wall and no attempt was made to shield the microphones from the turbulent boundary layer at the duct wall.

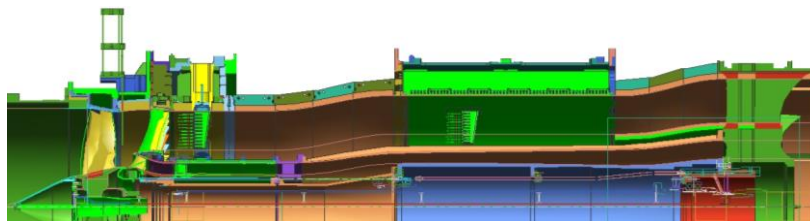


Figure 4. Schematic of the fan rig and measurement section in the bypass section

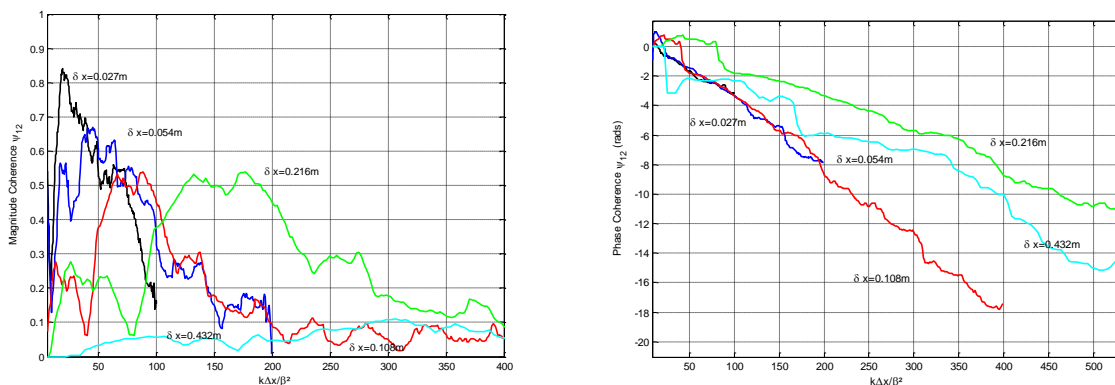


Figure 5 a and b show the magnitude and phase of the measured coherence for the five separation distances, $\Delta x = 0.027m, 0.054m, 0.108m, 0.216m,$ and $0.432m$, plotted against normalized separation distance.

The magnitude and phase of the coherence function are in reasonable agreement except for the two largest separation distances where the magnitude of the coherence is generally very small due to boundary layer noise. The corresponding inverted mode amplitude distribution function is shown below in figure 6.

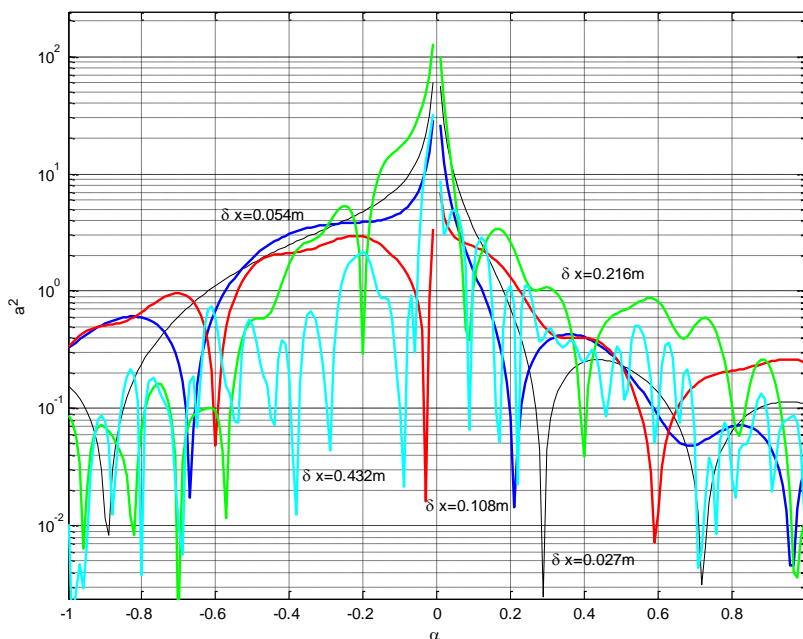


Figure 6. Modal amplitude distribution versus cutoff ratio deduced from the complex coherence function measured in the bypass section of a fan rig for 5 different separation distances.

As for the coherence estimates the mode amplitude estimates are reasonably consistent except for those obtained from the largest separation distances.

5. CONCLUSIONS

This paper has described a new method for determining the mode amplitude distribution in multi-mode broadband sound field in ducts in the presence of uniform mean flow and reflections. The novelty of the technique is that it requires only measurements of the complex coherence function made at the duct wall. The technique is valid in the high frequency limit and is restricted to cases where the relative mode amplitude distribution is independent of frequency.

REFERENCES

1. E. J. Rice 1978 *AIAA Journal*. **16**, 906–911 Multimodal far-field acoustic radiation pattern using mode cutoff ratio.
2. C.L. Morfey 1971 *Journal of Sound and Vibration* **14**, 37 – 55. Sound transmission and generation in ducts with flow.
3. E. J. Rice 1978 *AIAA Journal*. **16**, 906–911 Multimodal far-field acoustic radiation pattern using mode cutoff ratio.
4. P. Joseph, C.L. Morfey, C.R. Lewis. Multi-mode sound transmission in ducts with flow. *Journal of Sound and Vibration* 264 (2003) 523–544.
5. P. Joseph and C. L. Morfey 1999 *Journal of the acoustical society of America* **105**(5), 2590 - 2600. Multi-mode radiation from an unflanged, semi-infinite circular duct.
6. S. Sanyoko, P. Joseph and A. McAlpine. Multi-mode radiation from ducts with flow. *J. Acoust. Soc. Am.* 127 4, April 2010